JOURNAL OF MATERIALS SCIENCE **34** (1999) 1659–1665

A study on a $Ti_{52}Ni_{47}Al_1$ shape memory alloy

S. F. HSIEH, S. K. WU
Institute of Materials Science and Engineering, National Taiwan University, Taipei, Taiwan 106, Republic of China
E-mail: skw@ccms.ntu.edu.tw

The $Ti_{52}Ni_{47}Al_1$ alloy has 16% volume fraction Ti_2Ni particles in the B2 matrix with Ti_2Ni particles having a higher Al content than the B2 matrix. Transformation temperatures M^* and A^* of this alloy are lower than those of the $Ti_{51}Ni_{49}$ alloy due to the solid solution of the Al atoms. M^* and A^* decrease with increasing aging time at 400 °C because the Al atoms diffuse slightly from the Ti_2Ni to the B2 matrix. The hardness increment of this alloy is more than that of the $Ti_{51}Ni_{49}$ alloy under the same degree of cold rolling. At the same time, M^* and A^* of this alloy can be more depressed by thermal cycling than those of the $Ti_{51}Ni_{49}$ alloy, especially in the first ten cycles. All of these features result from the fact that this alloy has a higher inherent hardness due to the solid solution of the Al atoms. This also causes the R-phase transformation to be more easily promoted by both cold rolling and thermal cycling in this alloy. The strengthening effects of cold rolling and thermal cycling on the M^* (Ms) temperature of this alloy follows the expression $Ms = T_0 - K\Delta\sigma_y$, in which K values are affected by different strengthening processes. It is found that the higher the inherent hardness of the TiNi and TiNiX alloys, the higher the K values they have.

1. Introduction

Near-equiatomic TiNi alloys are the most important shape memory alloys (SMAs) because of their superior shape memory effect (SME) and pseudoelasticity (PE). TiNi alloys also have outstanding mechanical properties, biocompatibility and corrosion resistance. Substantial research has been conducted on the transformation behaviors and mechanical properties of TiNi binary alloys [1–4]. It has been confirmed that TiNi SMAs' properties can be affected by various thermomechanical treatments, such as thermal cycling [5], aging treatment in Ni-rich alloys [6–8] and cold rolling [9, 10]. The transformation sequence of TiNi SMAs can be B2 → B19′ or B2 → R → B19′ or simply B2 → R under different thermal mechanical processing techniques composed of a high temperature cubic B2 phase, a low temperature monoclinic B19′ phase and an intermediate rhombohedral R phase.

The transformation behaviors and shape memory characteristics of Ti-rich TiNi binary alloys have been reported under various thermo-mechancial treatment processes [11]. Small amounts of Ti replaced by Al in $Ti_{50}Ni_{50}$ SMA decreased the Ms temperature significantly [12]. However, there are few reports on ternary Ti-Ni-Al SMAs. The transformation behaviors and the microstructures of the R-phase in $Ti_{59.4}Ni_{38.7}Al_{1.9}$ alloy are affected by aging treatments [13, 14]. Additionally, the transformation sequence of Ni-rich $Ti_{49.5}Ni_{50.13}Al_{0.37}$ and $Ti_{47.5}Ni_{50.65}Al_{1.85}$ SMAs can be affected by the precipitates $Ti_{11}Ni_{14}$ during the aging [15]. To our best knowledge, the transformation behaviors and shape memory characteristics of Ti-rich Ti-Ni-Al alloys with near equiatomic Ti/Ni ratio have not yet been reported. It is the aim of the present work to systematically investigate the general characteristics of Ti-rich Ti-Ni-Al SMAs with near equiatomic Ti/Ni ratio. The transformation behaviors and shape recovery of these alloys will be compared to those of Ti-rich TiNi binary alloys. The effects of aging, cold rolling and thermal cycling on them will also be discussed.

2. Experimental procedure

The conventional tungsten arc melting technique was employed to prepare $Ti_{52}Ni_{47}Al_1$ and $Ti_{51}Ni_{48.5}Al_{0.5}$ alloys (in at %). Titanium (purity 99.7%), nickel (purity 99.9%) and aluminum (purity 99.9%), totaling about 120 g, were melted and remelted at least six times in an argon atmosphere. A pure titanium button was used as a getter during the arc melting. Weight loss during melting was negligibly small. The as-melted buttons were homogenized at 950 °C × 72 h and then quenched in water. The buttons were cut into several plates with a low speed diamond saw, and then solution-treated at 850 °C × 2 h and quenched in water. After the solution treatment, three experimental procedures were conducted. First, some plates were sealed in evacuated quartz tubes and aged at 400 °C for 1 to 240 h and then quenched in water. Second, some plates were cold-rolled at room temperature to 5, 10, 15 and 25% reduction in thickness. Third, other plates were subjected to thermal cycling N times from 0 to 200 °C with N = 1–100 cycles. Specimens for DSC measurements, hardness tests, shape recovery tests and microstructure observations were carefully cut from plates treated by the

above procedures. DSC measurements were made with a Dupont 9990 thermal analyzer equipped with a quantitative scanning system 910 DSC cell for controlled heating and cooling runs on samples encapsulated in an aluminum pan. The running temperature range was from $-50\,^{\circ}C$ to $+250\,^{\circ}C$ with a heating and cooling rate of $10\,^{\circ}C$/min. Specimens for the hardness test were first mechanically polished and then subjected to measurement in a microvickers hardness tester with 500 g load at room temperature. For each specimen, the average hardness value was taken from at least five test readings. The microstructure observations were made by optical microscope (OM). The shape recovery measurement was performed as described earlier by Lin and Wu [16]. A quantitative analysis of alloys' chemical composition was performed by using a JOEL JXA-8600SX electron probe microanalyzer (EPMA) equipped with WDX analysis system.

3. Experimental results and discussion

3.1. Transformation behavior in $Ti_{52}Ni_{47}Al_1$ alloy

Figs 1a and b show the experimental results of DSC measurements for the solution-treated $Ti_{52}Ni_{47}Al_1$ and $Ti_{51}Ni_{48.5}Al_{0.5}$ specimens in both forward and reverse transformations, respectively. The peaks M^* and A^* appearing in Fig. 1 are associated with the first order martensite transformation of B2 $\leftrightarrow$ B19′. The transformation behaviors of $Ti_{51}Ni_{48.5}Al_{0.5}$ alloy were found to be similar to those of the $Ti_{52}Ni_{47}Al_1$ alloy, therefore, experimental results and discussion of the former alloy are omitted in the rest of this paper.

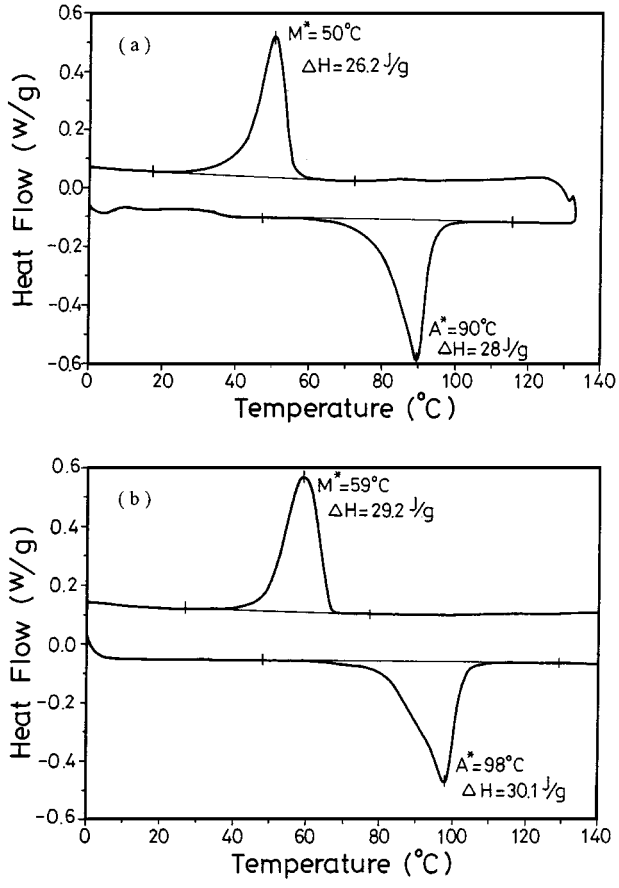

Figure 1 DSC curve for solution-treated (a) $Ti_{52}Ni_{47}Al_1$ alloy and (b) $Ti_{51}Ni_{48.5}Al_{0.5}$ alloy.

The transformation temperatures of $Ti_{52}Ni_{47}Al_1$ alloy are higher than those of equiatomic or Ni-rich TiNi alloys [6, 17], but lower than those of $Ti_{51}Ni_{49}$ alloy ($M^* = 70\,^{\circ}C$, $A^* = 110\,^{\circ}C$) [11]. It is reported [12] that the As temperature of TiNi binary alloys increases linearly as the Ti content increases up to 50.5 at % and then levels off at about $113\,^{\circ}C$. The ratio of Ti/Ni in the $Ti_{52}Ni_{47}Al_1$ alloy is 1.106, which is higher than that in the $Ti_{51}Ni_{49}$ alloy (1.041). Thus, the A^* and M^* temperatures of the $Ti_{52}Ni_{47}Al_1$ alloy are lower than those of the $Ti_{51}Ni_{49}$ alloy due to the aluminum atoms being solid-soluted in this alloy. However, this alloy still exhibits the same transformation sequence as Ti-rich TiNi alloys. Edmonds reported [13] that Al solid-soluted in TiNi alloy may result in different chemical free energy between various phases, in which the A^* and M^* temperatures can be depressed.

Based on Ti-Ni-Al ternary phase diagram at $900\,^{\circ}C$ [18], $Ti_{52}Ni_{47}Al_1$ alloy has a second phase Ti_2Ni to equilibrate with the B2 matrix. Fig. 2 shows the OM microstructure of this alloy. A great number of second phase particles are found around grain boundaries of the B2 matrix. The chemical compositions of the B2 matrix and Ti_2Ni particles by an EPMA analysis are shown in Table I. Table I indicates that Al atoms solid-soluted in Ti_2Ni particles are much more than those in the B2 matrix. Table I also shows that the hardness of Ti_2Ni particles is greater than that of the B2 matrix. The volume fraction of Ti_2Ni has been estimated by an image analyzer of OM to be about 16%.

Fig. 3 shows the shape memory characteristics of this alloy and the $Ti_{51}Ni_{49}$ alloy. The volume fraction of the Ti_2Ni in this alloy is much higher than that of the $Ti_{51}Ni_{49}$ alloy (about 10%). Despite the existence of many Ti_2Ni particles, the $Ti_{52}Ni_{47}Al_1$ alloy still exhibits good shape recovery which can reach $\cong$50% at the A_f temperature and gradually increase to $\cong$80% at $300\,^{\circ}C$. It is rather uncommon that the shape recovery gradually increases with increasing temperature at $T_{heating} \geq A_f$. Lin has reported [16] that the shape recovery of the equiatomic or Ni-rich TiNi alloys can reach $\cong$90% after heating to the A_f temperature and only minor recovery during subsequent heating. We believe that the above mentioned difference is closely related to the existence of Ti_2Ni particles and this phenomenon also occurs in $Ti_{51}Ni_{49}$ alloy. From Fig. 3, one can also find that the shape recovery of this alloy is much better than

TABLE I The composition and hardness of matrix and Ti_2Ni in thermomechanical-treated $Ti_{52}Ni_{47}Al_1$ alloy

	Solution treatment		$400\,^{\circ}C \times 240$ h aging treatment	
	Matrix	Ti_2Ni	Matrix	Ti_2Ni
Ti (at %)	50.71	65.35	50.79	65.25
Ni (at %)	48.43	32.44	48.27	32.59
Al (at %)	0.86	2.21	0.94	2.16
Hardness (Hv)	235	268	250	265

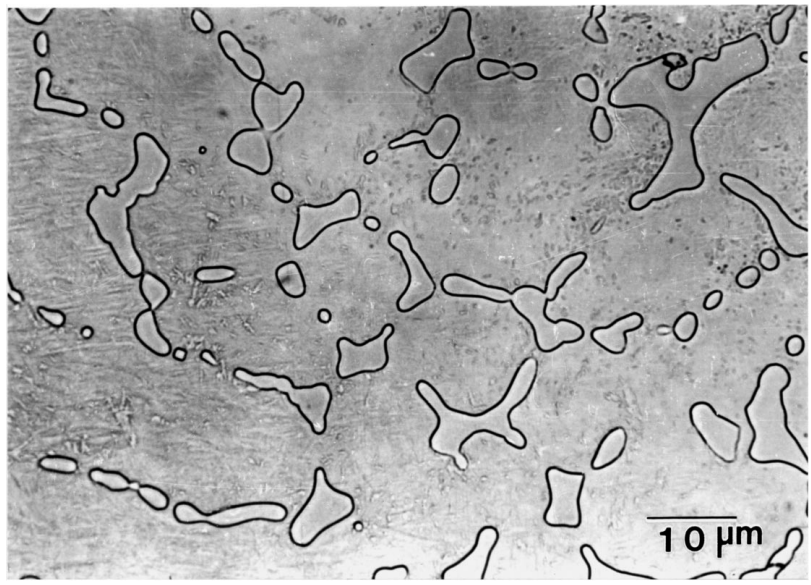

Figure 2 OM microstructures of solution-treated $Ti_{52}Ni_{47}Al_1$ alloy.

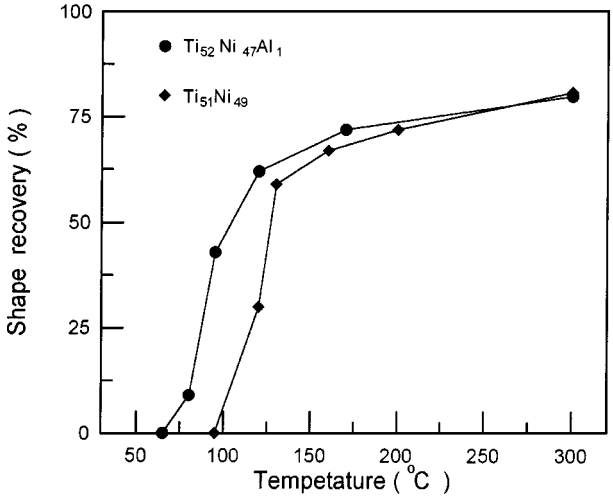

Figure 3 Shape recovery vs. heating temperature for $Ti_{52}Ni_{47}Al_1$ and $Ti_{51}Ni_{49}$ alloys.

that of $Ti_{51}Ni_{49}$ alloy below 130 °C, but exhibits equal behavior above 200 °C. This feature results from the solid-solution hardening obtained by Al solid-soluted in the B2 matrix of the $Ti_{52}Ni_{47}Al_1$ alloy, as shown in Table I. Although the quantity of Ti_2Ni particles in this alloy is much higher than that in the $Ti_{51}Ni_{49}$ alloy, this feature also explains the reason why the shape recovery of this alloy does not decrease substantially.

3.2. Aging effect on $Ti_{52}Ni_{47}Al_1$ alloy

The DSC measurements for the 400 °C aged $Ti_{52}Ni_{47}Al_1$ specimens show that the transformation sequence is B2 → B19′ martensitic transformation and the experimental A^* and M^* temperatures are plotted in Fig. 4a. The A^* and M^* temperatures gradually decrease with increasing aging time at 400 °C. The chemical composition of Ti_2Ni particles and the B2 matrix by EPMA analysis for 400 °C × 240 h aged specimen is also shown in Table I. From Table I, Al atoms are found to diffuse from the higher Al-content of Ti_2Ni particles to the lower one of the B2 matrix. Therefore, Al atoms soluted in the B2 matrix increase slightly during the aging at 400 °C. This feature results in the decrease of A^* and M^* temperatures and the increase of matrix hardness during the aging. It has been reported that the shape recovery of TiNi alloys can be increased by different thermo-mechanical strengthening treatments [16].

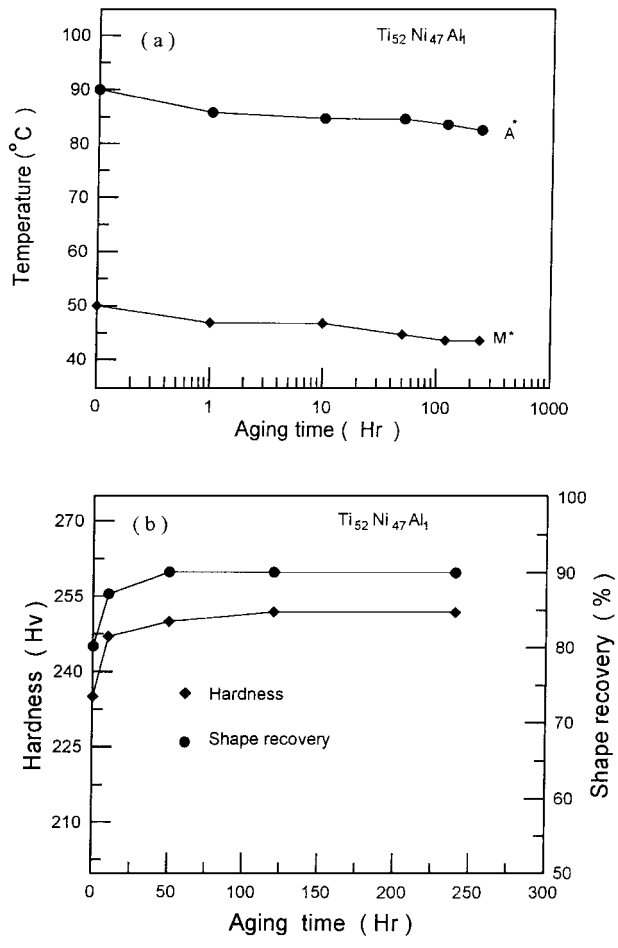

Figure 4 (a) A^* and M^* temperature, (b) shape recovery and hardness, vs. aging time for $Ti_{52}Ni_{47}Al_1$ alloy.

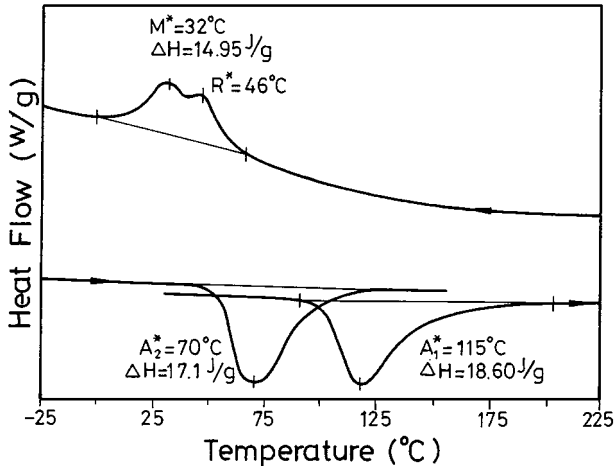

Figure 5 DSC curve for 5% cold-rolled $Ti_{52}Ni_{47}Al_1$ alloy.

Therefore, the shape recovery of this alloy can also increase during the aging because Al atoms diffuse into the B2 matrix and cause the matrix to be harder, as shown in Fig. 4b. The shape recovery can reach ≅90% for the specimens aged at more than 60 h at 400 °C.

3.3. Cold rolling effect on $Ti_{52}Ni_{47}Al_1$ alloy

The effects of cold rolling on the martensite transformation of equiatomic TiNi binary alloy have been systematically studied. The phenomenon of martensite stabilization was observed in the cold rolled TiNi martensite [17]. In this study, the $Ti_{52}Ni_{47}Al_1$ alloy underwent plastic deformation when cold-rolled at room temperature. Fig. 5 shows the DSC curve for the 5% cold-rolled $Ti_{52}Ni_{47}Al_1$ alloy. In Fig. 5, peak A_1^* appears at +115 °C on the first heating cycle from room temperature to +250 °C. The duplex peak appears on the following cooling cycle from +250 °C to −50 °C in which M^* is at +32 °C and R^* (B2 → premartensite R-phase) is at +46 °C. Peak A_2^* appears at +70 °C on the second heating cycle from −50 to +250 °C. Peaks A_1^*, M^* and A_2^* are all associated with the martensitic transformation. The DSC curves for other cold-rolled specimens (10–25%) similar to that shown in Fig. 5 and therefore are omitted here. The peak A_1^* temperature signficantly increases with an increasing degree of cold-rolling. This feature exhibits the phenomenon of martensite stabilization, as that observed in the cold-rolled equiatomic TiNi and $Ti_{51}Ni_{49}$ alloys [11, 17]. After the occurrence of the first reverse martensitic transformation of B19′ → B2, the martensite stabilization dies out and A_2^* temperatures are lower than A_1^* temperatures. In Fig. 6a, the difference between peak temperature A_1^* and A_2^*, ΔA^*, stands for the degree of martensite stabilization. From Fig. 6a, the ΔA^* of the $Ti_{52}Ni_{47}Al_1$ alloy ($\Delta A^* = 89$ °C) is larger than that of the equiatomic TiNi alloy ($\Delta A^* = 82$ °C) [19] and $Ti_{51}Ni_{49}$ alloy ($\Delta A^* = 84$ °C) [11] for the same 25% cold-rolled specimen. Fig. 6b shows the increment of hardness at the same degree of cold rolling is about 150 Hv for the $Ti_{52}Ni_{47}Al_1$ alloy, which is larger than that of TiNi alloy (ΔHv = 136) [19] and $Ti_{51}Ni_{49}$ alloy (ΔHv = 143) [11]. This feature results from the as-solid-soluted $Ti_{52}Ni_{47}Al_1$ alloy being harder than

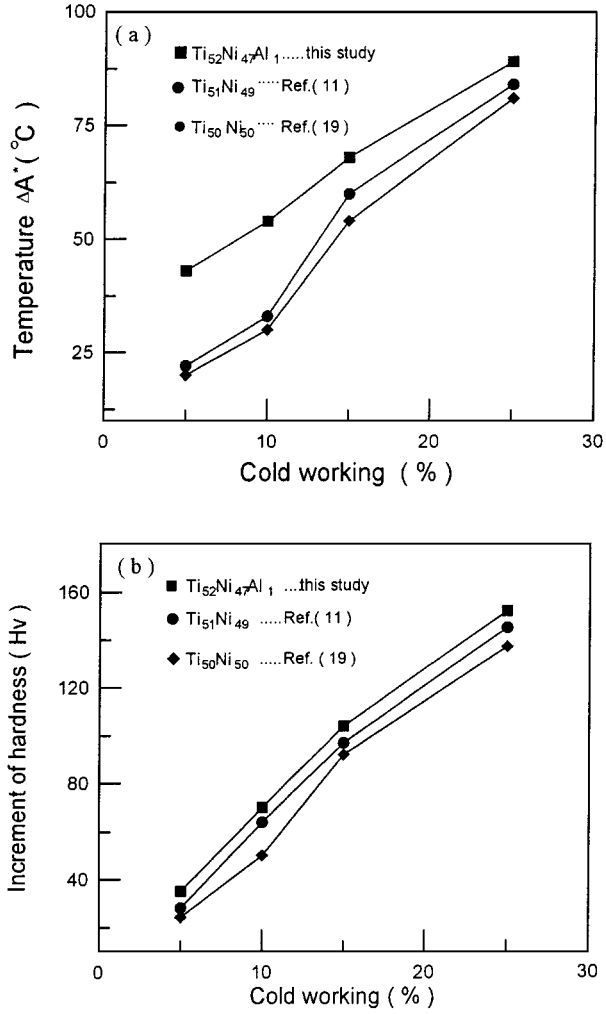

Figure 6 (a) The degree of martensite stabilization (ΔA^*) and (b) the increment of hardness (ΔHv) vs. degree of cold rolling for the $Ti_{52}Ni_{47}Al_1$ alloy.

the equiatomic TiNi and $Ti_{51}Ni_{49}$ alloys, as shown in Table II. At the same time, the dislocation/defect movement can be more hindered by harder Ti_2Ni particles during plastic deformation in the $Ti_{52}Ni_{47}Al_1$ alloy. Hence, the harder $Ti_{52}Ni_{47}Al_1$ alloy has a higher increment of hardness and a higher degree in martensite stablization under the same degree of cold rolling, as shown in Fig. 6.

The DSC curve for $Ti_{51}Ni_{49}$ alloy cold-rolled at more than 20% in thickness appears the duplex peak in the cooling curve. However, as shown in Fig. 5, the R-phase can be induced in the 5% cold-rolled $Ti_{52}Ni_{47}Al_1$ specimen. This feature shows that the R-phase can be

TABLE II The K value for different strengthening process and the solution-treated hardness of TiNi shape memory alloys

Composition (in at %)	Solution-treated hardness (Hv)	K value	
		Thermal cycling	Cold rolling
$Ti_{50}Ni_{50}$	200	0.52	0.28
$Ti_{51}Ni_{49}$	228	0.62	0.42
$Ti_{52}Ni_{47}Al_1$	235[a]	0.65	0.44
$Ti_{41.5}Ni_{48.5}Zr_{10}$	285	0.68	0.58

[a] The hardness of solution-treated in B2 matrix.

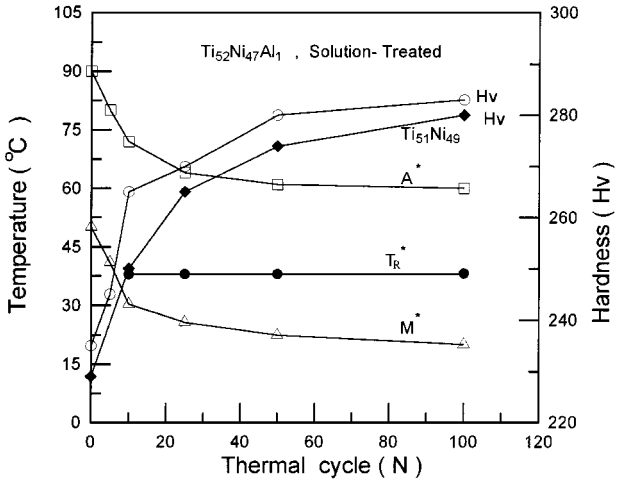

Figure 7 Hardness and peak temperatures of A_1^*, M^*, and R^* vs. number of thermal cycles (N) for solution-treated $Ti_{52}Ni_{47}Al_1$ alloy.

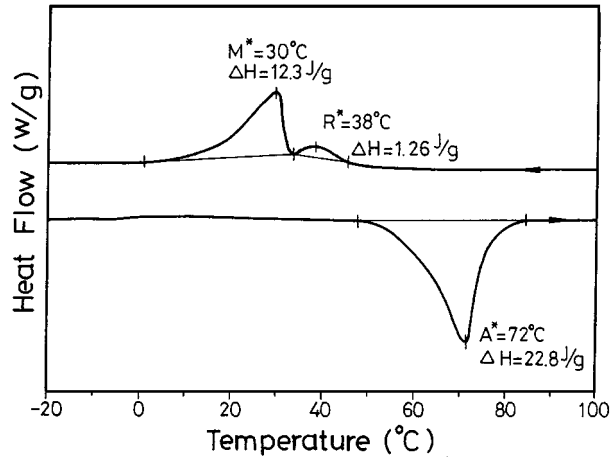

Figure 8 DSC curve for thermal cycled $Ti_{52}Ni_{47}Al_1$ alloy at $N = 10$.

promoted by Al atoms soluted in TiNi alloys, a behavior similar to Fe soluted in TiNi alloys [20]. In our previous study on Ni-rich $Ti_{49.5}Ni_{50.13}Al_{0.37}$ and $Ti_{47.5}Ni_{50.65}Al_{1.85}$ alloys [15], it was also found that the solid-soluted Al atoms in these two alloys can also induce R-phase transformation.

3.4. Thermal cycling effects on $Ti_{52}Ni_{47}Al_1$ alloy

Fig. 7 shows peak temperatures M^*, A^* and hardness Hv vs. thermal cycle N for solution-treated $Ti_{52}Ni_{47}Al_1$ alloy. In Fig. 7, the M^* and A^* temperatures decrease, but the hardness Hv with increasing thermal cycling. It has been proposed that this feature comes from the dislocations induced by thermal cycling [3]. The A^* and M^* decrease quickly for the first ten cycles with the decrement being about 18 °C at $N = 10$, which is larger than that of $Ti_{51}Ni_{49}$ alloy ($\cong$10 °C) [21]. The increase in hardness of this alloy ($\Delta Hv = 29$) is also greater than that of the $Ti_{51}Ni_{49}$ alloy ($\Delta Hv = 23$) at the same $N = 10$ cycles. This indicates that $Ti_{52}Ni_{47}Al_1$ alloy can induce many more dislocations than can the $Ti_{51}Ni_{49}$ alloy in the early thermal cycling. We suggest that the volume change during the martensitic transformation can produce a complex stress field at the interface of Ti_2Ni particles and B2/B19′ matrix during thermal cycling. This complex stress field can enhance the dislocation multiplication, which increases the hardness of the alloy and depresses its M^* temperature. Fig. 8 shows that the R-phase transformation can also be promoted by the early ten cycles. Compared with $Ti_{51}Ni_{49}$ alloy, which needs more than $N \cong 100$ cycles to appear the R-phase transformation [21], we suggest that $Ti_{52}Ni_{47}Al_1$ alloy is easier to promote R-phase appearing than $Ti_{51}Ni_{49}$ alloy during thermal cycling. In Fig. 7, after 50 cycles, the M^* and A^* temperatures reach a constant value. This may indicate that the quantities of induced dislocations reach a saturated value after 50 cycles in $Ti_{52}Ni_{47}Al_1$ alloy.

The cold-rolled $Ti_{52}Ni_{47}Al_1$ specimens with 5 and 25% thickness reduction have also been subjected to thermal cycling tests, as shown in Fig. 9. For 5% cold-rolled specimen, A^* and M^* temperatures are depressed

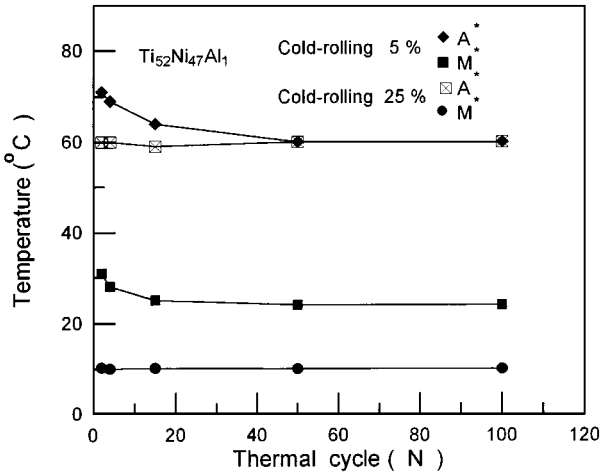

Figure 9 Peak temperatures A^* and M^* of 5%, 25% cold-rolled $Ti_{52}Ni_{47}Al_1$ alloy vs. number of thermal cycles.

to lower temperatures as N increases, althougth the depression is less than in those of Fig. 7. This feature comes from the fact that 5% cold rolling can introduce dislocations and strengthen the alloy. Therefore, only a small quantity of extra dislocations can be induced during thermal cycling. This elucidates that the 5% cold-rolled specimen exhibits only a few of the effects of thermal cycling. If the degree of cold rolling reaches 25%, the specimen has been signficantly strengthened by cold rolling and the extra dislocations are difficult to be induced during thermal cycling. Hence, for this heavy cold-rolled specimen, transformation temperatures keep nearly the same values even when the thermal cycling N reaches 100 cycles, as shown in Fig. 9.

3.5. Strengthening effects of cold-rolling and thermal cycling on martensitic transformation temperatures of $Ti_{52}Ni_{47}Al_1$ alloy

Figs 10a and b show the curves of peak temperature M^* vs. hardness Hv for the cold-rolled and thermal-cycled $Ti_{52}Ni_{47}Al_1$ alloy, respectively. The results of cold-rolled and thermal-cycled $Ti_{50}Ni_{50}$ and Ti-rich $Ti_{51}Ni_{49}$ alloys are also shown in Fig. 10. It was pointed out that

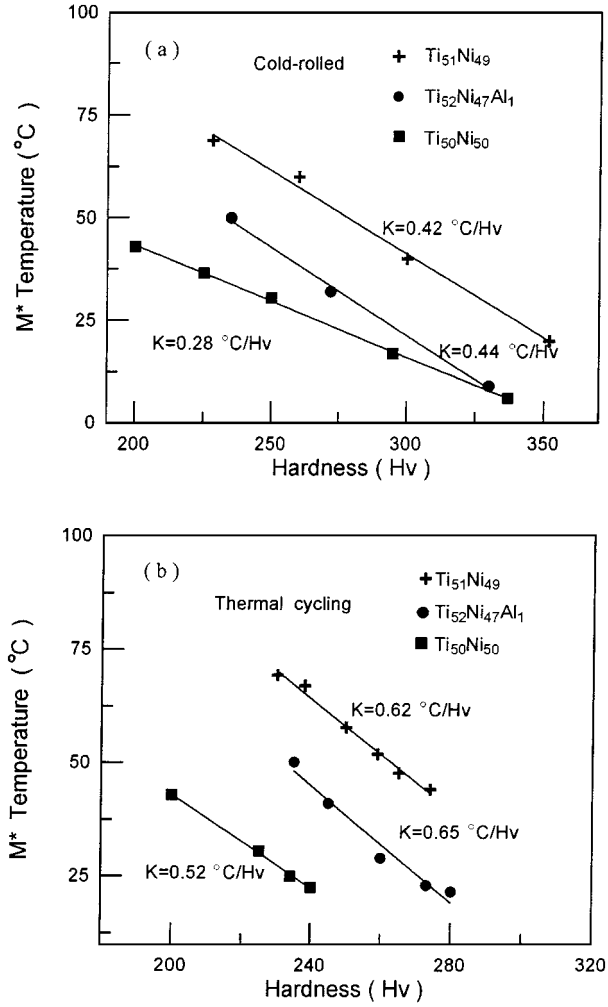

Figure 10 M^* temperature vs. hardness for (a) cold-rolled and (b) thermal cycled $Ti_{50}Ni_{50}$, $Ti_{51}Ni_{49}$ and $Ti_{52}Ni_{47}Al_1$ alloys.

any strengthening mechanism which impedes the transformation shear can lower the transformation temperatures because the martensitic transformation involves a shear process [22, 23]. This feature can be expressed by the Equation 1.

$$\mathrm{Ms} = T_0 - K\Delta\sigma_y \quad (1)$$

where the constant K contains the factors of proportionality between the critical shear stress and the yield stress $\Delta\sigma_y$, the equilibrium temperature T_0 is a function of the chemical composition, and the yield stress $\Delta\sigma_y$ is regarded as proportional to the hardness.

In this study, both cold-rolling and thermal cycling do not change the alloy's composition, hence T_0 is a constant. In addition, both cold rolling and thermal cycling can strengthen the alloys by inducing dislocations, and therefore can raise the yield stress $\Delta\sigma_y$. As derived from Equation 1, this feature should cause the M^* and A^* temperatures to be lowered by the strengthening effect. This prediction is qualitatively consistent with the results of Fig. 10. In Fig. 10, the slope represents the constant K which is not the same for different strengthening processes. These results indicate that processes of cold rolling and thermal cycling can provide different strengthening mechanisms and exhibit different effects on transformation temperatures. As mentioned above, strengthening processes can introduce dislocations in these alloys. However, dislocations induced by cold rolling come from the plastic deformation of martensite and those induced by thermal cycling come from the thermal stress and transformation shear associated with B2 $\rightarrow$ B19′. Carefully examine Fig. 10, the constant K of $Ti_{52}Ni_{47}Al_1$ alloy is larger than that of $Ti_{50}Ni_{50}$ and $Ti_{51}Ni_{49}$ alloys for the same strengthening process. We propose that the K value is related to the inherent hardness of solution-treated TiNi binary or TiNiX ternary alloys. The higher the original hardness, the larger the K value is. For example, as can be seen from Table II, the thermal cycled $Ti_{41.5}Ni_{48.5}Zr_{10}$ alloy has its solution-treated hardness at about 285 Hv and its K value is found to be 0.68 °C/Hv [24], which is larger than those of thermal cycled $Ti_{51}Ni_{49}$ and $Ti_{50}Ni_{50}$ alloys in Fig. 10. In other words, the depression of Ms (M^*) and As (A^*) temperatures by the strengthening mechanism is stronger for the alloys having a higher solution-treated hardness. This also elucidates the reason why the K value of the $Ti_{52}Ni_{47}Al_1$ alloy is higher than those of the $Ti_{50}Ni_{50}$ and $Ti_{51}Ni_{49}$ alloys under the same strengthening process, as shown in Fig. 10. From Fig. 10, it can also be seen that the thermal cycled K value is larger than the cold-rolled one for each of the equiatomic TiNi, $Ti_{51}Ni_{49}$ and $Ti_{52}Ni_{47}Al_1$ alloys. These results mean that the strengthening effect of thermal cycling is larger than that of cold rolling for TiNi SMAs.

4. Conclusion

1. The solution-treated $Ti_{52}Ni_{47}Al_1$ alloy undergoes the first order B2 $\rightarrow$ B19′ martensitic transformation. Many second phase Ti_2Ni particles with a 16% volume fraction are found at the grain boundaries of the B2 matrix in which Al atoms are much more solid-soluted in Ti_2Ni particles than in the B2 matrix. Transformation temperatures A^* and M^* of this alloy are higher than those of equiatomic or Ni-rich TiNi alloys, but lower than those of $Ti_{51}Ni_{49}$ alloy due to Al atoms being solid-soluted in the B2 matrix.

2. A^* and M^* temperatures of this alloy decrease slightly with increasing aging time at 400 °C because Al atoms diffuse from Ti_2Ni particles to the B2 matrix. At the same time, the shape recovery and hardness of this alloy increase with increasing aging time due to the Al atoms solution hardening in the B2 matrix.

3. Martensite stabilization of this alloy can be induced by cold rolling at room temperature. The hardness increment of this alloy is more than that of equiatomic and $Ti_{51}Ni_{49}$ alloys under the same degree of cold rolling. In addition, 5% thickness reduction is enough to promote R-phase transformation in this alloy, but it needs at least 20% for $Ti_{51}Ni_{49}$ alloy. Al atoms solid-soluted in TiNi alloys are suggested to account for these characteristics.

4. A^* and M^* temperatures decrease and the hardness increases quickly in the first ten cycles of thermal cycled $Ti_{52}Ni_{47}Al_1$ alloy. Meanwhile, the decrement of A^* temperatures of this alloy is larger than that of $Ti_{51}Ni_{49}$ alloy at the same N. R-phase transformation can also be more easily promoted in the thermal cycled

$Ti_{52}Ni_{47}Al_1$ alloy. Dislocations more easily induced by thermal cycling in this alloy can account for these features. For 25% cold-rolled $Ti_{52}Ni_{47}Al_1$ alloy, M^* and A^* are found to be nearly unaffected by the thermal cycling.

5. The strengthening effects of cold-rolling and thermal cycling on Ms (M^*) temperatures of $Ti_{52}Ni_{47}Al_1$ alloy are found to follow the equation $Ms = T_0 - K\Delta\sigma_y$. Strengthening processes of cold rolling and thermal cycling have their different K values. Experimental results show that K values are associated with the inherent hardness of TiNi alloys. The $Ti_{52}Ni_{47}Al_1$ alloy has Al atoms solid-soluted in it and has a higher original hardness than the $Ti_{51}Ni_{49}$ alloy, and thus has a higher K value.

Acknowledgement

The authors sincerely acknowledge the financial support of this study by the National Science Council (NSC), Republic of China, under Grant NSC 83-0405-E002-029.

References

1. G. D. SANDROCK, J. A. PEKINS and R. F. HEHENMANN, *Metall. Trans.* **2A** (1971) 2769.
2. H. C. LING and R. KAPOW, *ibid.* **12A** (1981) 2102.
3. S. MIYAZAKI, T. IMAI, Y. IGO and K. OTSUKA, *ibid.* **17A** (1986) 115.
4. S. MIYAZAKI, Y. OHMI, K. OTSUKA and Y. SUZUKI, (ICOMAT-82), *J. de Phys.* **43** (1982) C4-255.
5. S. MIYAZAKI, Y. IGO and K. OTSUKA, *Acta Metall.* **34** (1986) 2045.
6. S. K. WU, H. C. LIN and T. S. CHOU, *ibid.* **38** (1990) 95.
7. M. NISHIDA and T. HONMA, *Scripta Metall.* **18** (1984) 1293.
8. *Idem. ibid.* **18** (1984) 1389.
9. Y. OKAMOTO, H. HAMANAKA, F. MIURA, H. TAMURA and H. HORIKAWA, *ibid.* **22** (1988) 517.
10. T. TODOROKI and H. TAMURA, *Trans. JIM.* **28** (1987) 83.
11. H. C. LIN, S. K. WU and J.C. LIN, *Materials Chemistry and Physics* **37** (1994) 184.
12. K. H. ECKELMEYER, *Scripta Metall.* **10** (1976) 667.
13. K. R. EDMONDS and C. M. HWANG, *ibid.* **20** (1986) 733.
14. C. M. HWANG and C. M. WAYMAN, *Metall. Trans.* **15A** (1984) 1155.
15. S. F. HSIEH and S. K. WU, *J. Mater. Sci.* **32** (1997) 989.
16. H. C. LIN and S. K. WU, *Scripta Metall.* **26** (1992) 59.
17. H. C. LIN, S. K. WU, T. S. CHOU and H.P. KAO, *Acta Metall.* **39** (1991) 2069.
18. K. J. LEE and P. NASH, *J. of Phase Equilibria* **12** (1991) 551.
19. H. C. LIN, PhD thesis, Institute of Materials Science and Engineering, National Taiwan University, Taipei, Taiwan, 1992.
20. C. M. HWANG, M. MEICHLE, M. B. SALAMON and C. M. WAYMAN, *Phil. Mag.* **47** (1983) 9, 31, 177.
21. J. C. LIN, Masters' thesis, Institute of Materials Science and Engineering, National Taiwan University, Taipei, Taiwan, 1991.
22. M. COHEN, E. S. MACHLIN and V. G. PARANJPE, "Thermodynamics in Physical Metallurgy" (ASM, Metals Park, OH, 1950).
23. E. HORNBOGEN, *Acta Metall.* **33** (1991) 595.
24. S. H. CHEN, Masters' thesis, Institute of Materials Science and Engineering, National Taiwan University, Taipei, Taiwan, 1994.

Received 15 January 1997
and accepted 6 October 1998